The Journal of Chemical Physics

Computational modeling of charge hopping dynamics along a disordered one-dimensional wire with energy gradients in quantum environments

Cite as: J. Chem. Phys. **153**, 054109 (2020); https://doi.org/10.1063/5.0011004
Submitted: 17 April 2020 . Accepted: 08 July 2020 . Published Online: 04 August 2020

Ning Chen, Murali Devi, and Seogjoo J. Jang

View Online Export Citation CrossMark

Lock-in Amplifiers up to 600 MHz Watch

© 2020 Author(s).

The Journal of Chemical Physics ARTICLE scitation.org/journal/jcp

Computational modeling of charge hopping dynamics along a disordered one-dimensional wire with energy gradients in quantum environments

Cite as: J. Chem. Phys. 153, 054109 (2020); doi: 10.1063/5.0011004
Submitted: 17 April 2020 • Accepted: 8 July 2020 •
Published Online: 4 August 2020

View Online Export Citation CrossMark

Ning Chen,[1,2] Murali Devi,[1,3] and Seogjoo J. Jang[1,2,a)]

AFFILIATIONS

[1] Department of Chemistry and Biochemistry, Queens College, City University of New York, 65-30 Kissena Boulevard, Queens, New York 11367, USA
[2] Chemistry and Physics Ph.D. Programs and Initiative for Theoretical Sciences, Graduate Center, City University of New York, 365 5th Ave., New York, New York 10016, USA
[3] Department of Physics, St. John's University, 8000 Utopia Pkwy, Jamaica, New York 11439, USA

[a)] **Author to whom correspondence should be addressed:** sjang@qc.cuny.edu

ABSTRACT

This computational study investigates the effects of energy gradients on charge hopping dynamics along a one-dimensional chain of discrete sites coupled to quantum bath, which is modeled at the level of Pauli master equation (PME). This study also assesses the performance of different approximations for the hopping rates. Three different methods for solving the PME, a fourth order Runge–Kutta method, numerical diagonalization of the rate matrix followed by analytic propagation, and kinetic Monte Carlo simulation method, are tested and confirmed to produce virtually identical values of time dependent mean square displacement, diffusion constant, and mobility. Five different rate expressions, exact numerical evaluation of Fermi's Golden Rule (FGR) rate, stationary phase interpolation (SPI) approximation, semiclassical approximation, classical Marcus rate, and Miller–Abrahams rate, are tested to help understand the effects of approximations in representing quantum environments in the presence of energy gradients. The results based on direct numerical evaluation of FGR rate exhibit transition from diffusive to non-diffusive behavior with the increase in the gradient and show that the charge transport in the quantum bath is more sensitive to the magnitude of the gradient and the disorder than in the classical bath. Among all the four approximations for the hopping rates, the SPI approximation is confirmed to work best overall. A comparison of two different methods to calculate the mobility identifies drift motion of the population distribution as the major source of non-diffusive behavior and provides more reliable information on the contribution of quantum bath.

Published under license by AIP Publishing. https://doi.org/10.1063/5.0011004

I. INTRODUCTION

Efficient charge transport (CT) in conjugated organic materials is a central issue in the development of organic light-emitting diodes, field-effect transistors, and photovoltaic solar cells.[1–6] The major benefit of organic materials is their relative low cost and good processability.[4–8] However, complex vibrational modes and distortion of molecules in conjugated organic materials tend to result in environments that are unfavorable for charge transport in comparison to traditional inorganic materials. In this regard, how to control and enhance CT in organic materials, even in the presence of significant disorder, remains an important subject of theoretical investigation.

In contrast to the band theory mechanism of CT dynamics typically assumed in inorganic materials, CTs in organic materials are believed to involve mainly hopping mechanisms.[4,9] This is due to relatively weak electronic couplings between different charge centers compared to electron–phonon interactions.[4,10] The assumption

Published under license by AIP Publishing

of hopping mechanism rules out the possibility of coherent quantum transfer, which is significant in systems with weak electron–phonon interactions,[11] but can still account for other incoherent quantum effects. In the end, calculations based on first principles and/or advanced quantum dynamics methods[12–16] may be needed for reliable assessment of CT mechanisms and quantitative modeling. However, considering limited computational capability and the large scale of systems to investigate, coarse-grained simulation of the dynamics with some phenomenological component, for example, employing the Pauli master equation (PME), has great practical utility for modeling CT processes.[17–21]

One important component in coarse-grained simulation of CT is the specification of the type of disorder resulting from uncontrollable microscopic factors. Independent Gaussian disorder model (GDM) has been widely used for the simulation of CT processes[10] in dilute charge density limits, whereas the correlated disorder model has been advocated more[22,23] for high charge density limits. Thus, for applications to photovoltaic devices where the charge carrier density is low, the assumption of GDM seems reasonable. GDM has also been tested broadly by the kinetic Monte Carlo (KMC) simulation method,[10,24–26] which offers an efficient way to simulate the solution of PME for the hopping dynamics.

The PME provides a general framework to describe a broad range of hopping dynamics and has been used by many groups for the computational study of CT in systems of conjugated organic molecules.[18,26–30] However, there are still many microscopic features that need to be clarified for quantitatively reliable PME calculation of CT processes in conjugated organic materials. The CT mechanism in these systems is complicated due to intricate interactions of charge carriers and the thermal bath. Temperature also plays a crucial role in altering the transfer mechanism. In the high temperature limit, thermally induced hopping can be the major mechanism. In the low temperature limit, nuclear tunneling can become pronounced, and more vibrational modes need to be treated quantum mechanically. The range of temperature where the transition between the two limits occurs is not clearly known for many systems.

In particular, nuclear quantum effect[1,3,18,31] can play a crucial role in CT in conjugated organic materials, where there are many vibrational/phonon modes with level spacings larger than thermal energy.[3] In order to investigate the contribution of nuclear quantum effects, direct evaluation of Fermi's Golden Rule (FGR) rate expression is necessary in general. However, this is not always feasible especially in large scale systems, for which approximations need to be employed instead. A relatively new approximation that can be useful in this respect is the stationary phase interpolation (SPI) approximation developed by Jang and Newton,[32] which has been tested and compared in a previous computational study in the absence of energy gradients.[33] More recently, different kinds of approximations including nonequilibrium and non-Condon effects have also been developed by Geva and co-workers.[34–37]

The primary focus of the present work is to understand the effects of the gradient in site energies on the CT dynamics in disordered quantum environments. The gradient in this case mimics the effect of the external field. In general, the applied field can cause complicated local effects[4] such as re-orientation of dipoles, displacement of charge carriers, and collective responses such as induced polarizations. However, to the extent that the linear constitutive relationship holds,[38] the net effect of those perturbations can be modeled by a linear gradient in site energies. Even in this case, the dynamical effect of such gradients can be significant, causing non-diffusive behavior in some cases. Simulations for a series of different values of gradients can help gain more quantitative understanding of how these features emerge and the performance of different approximations in capturing those features.

The paper is organized as follows. Section II describes the theoretical model and computational methods. Section III provides results of calculation and discussion. Conclusion is provided in Sec. IV.

II. THEORETICAL MODEL AND COMPUTATIONAL METHOD

A. Model and Pauli master equation

We conduct simulation of charge hopping dynamics for a model of one-dimensional wire with N sites in the presence of Gaussian energetic disorder and a gradient in average site energies. The coordinate and free energy for the nth site are denoted as r_n and G_n, respectively. This site free energy consists of two components as follows:

$$G_n = G_n^0 + \delta G_n, \tag{1}$$

where G_n^0 is the intrinsic free energy at the nth site and is assumed to be randomly drawn from the following Gaussian distribution:

$$g(G) = \frac{1}{\sqrt{2\pi\sigma^2}} \exp\left(-\frac{G^2}{2\sigma^2}\right). \tag{2}$$

In the above expression, σ is the standard deviation of the Gaussian distribution for the site free energy. The second term δG_n in Eq. (1) is a perturbation defined by

$$\delta G_n = -er_nF, \tag{3}$$

where e is the charge of electron and F is the net electric field assumed to be uniform across the wire. Thus, the charge carrier is assumed to be an electron. Positive sign needs to be used in case hole becomes the charge carrier. Employing Eqs. (1) and (3), the free energy difference between two sites can be expressed as

$$\Delta G_{mn}(F) = \Delta G_{mn}^0 - er_{mn}F, \tag{4}$$

where $\Delta G_{mn}^0 = G_m^0 - G_n^0$ is the free energy difference between sites m and n for $F = 0$ and $r_{mn} = r_m - r_n$ is the displacement between the two sites. Note that F is different from the applied field and includes the effect of the local induced electric field.

The PME describing the time evolution of $P_n(t)$, the population of the charge carrier at site n at time t, is expressed as

$$\frac{dP_m(t)}{dt} = \sum_{n=1,n\neq m}^{N} \{k_{n\to m}P_n(t) - k_{m\to n}P_m(t)\}, \tag{5}$$

where $k_{n\to m}$ is the hopping rate from site n to site m. In this work, it is assumed that the hopping occurs only between the nearest neighbors. Thus, $k_{n\to m}$ is nonzero only for $m = n \pm 1$; for the boundary points, this applies to only one direction because only $k_{1\to 2}$ and $k_{N\to N-1}$ are defined. The above PME does not account for

Published under license by AIP Publishing

correlation of charge carrier populations and is thus valid only for the weak charge carrier density limit.

B. Microscopic model and rate expressions

For the hopping rates, we use the same set used in a previous study,[33] namely, exact numerical evaluation of FGR, the Marcus rate,[40,41] a conventional semiclassical (SC) approximation,[42] the SPI approximation,[32] and the Miller–Abrahams (MA) rate.[39] Before providing these expressions, let us first consider the following microscopic model Hamiltonian (for each realization of disorder) that generalizes the spin-boson type Hamiltonian[57] for multisite situation:

$$\hat{H}_\xi = \sum_{n=1}^{N} G_n(\xi)|n\rangle\langle n| + \sum_{n=1}^{N-1} J(|n\rangle\langle n+1| + |n+1\rangle\langle n|) + \sum_r \hbar\omega_r g_{n,r}(\hat{b}_r + \hat{b}_r^\dagger) + \sum_r \hbar\omega_r\left(\hat{b}_r^\dagger\hat{b}_r + \frac{1}{2}\right), \tag{6}$$

where ξ represents each collection of the disorder in G_n's, J is the electronic coupling between neighboring sites, and $\hat{b}_r$ ($\hat{b}_r^\dagger$) is the lowering (raising) operator for a harmonic oscillator normal mode with frequency ω_r. The set of these normal modes coupled linearly to charge localized states $|n\rangle$'s represents the environmental degrees of freedom responding to CT, which also include the contribution of intra-molecular vibrational modes. Note that the free energy is used for each site in the above equation. This is due to the coarse-grained nature of the model. However, it is also important to note that the contribution of the environments modeled by the harmonic oscillators is excluded from this calculation of free energy.

We assume that the environmental responses of all sites are equivalent. Thus, their primary effects on CT between each neighboring site can be characterized by the following spectral density:

$$\mathcal{J}(\omega) = \pi\hbar\sum_r \delta(\omega-\omega_r)\omega_r^2(g_{n,r}-g_{n+1,r})^2, \tag{7}$$

where the set of indices r's is structured such that the right-hand side (after the summation) becomes independent of n. Note that the above spectral density is defined in the standard manner,[58] which is different from the one used in a previous work.[33]

For the spectral density defined above, the classical reorganization energy λ that enters the Marcus rate expression[40,41] is expressed as follows:

$$\lambda = \frac{1}{\pi}\int_0^\infty d\omega\frac{\mathcal{J}(\omega)}{\omega}. \tag{8}$$

On the other hand, three quantum reorganization energies that appear in stationary phase approximations[32] can be defined as follows:

$$\lambda_{q,c} = \frac{\hbar}{2\pi k_B T}\int_0^\infty d\omega\mathcal{J}(\omega)\coth\left(\frac{\hbar\omega}{2k_BT}\right), \tag{9}$$

$$\lambda_{q,s} = \frac{\hbar}{2\pi k_B T}\int_0^\infty d\omega\mathcal{J}(\omega)\mathrm{csch}\left(\frac{\hbar\omega}{2k_BT}\right), \tag{10}$$

$$\lambda_{q,t} = \frac{4k_BT}{\pi\hbar}\int_0^\infty d\omega\frac{\mathcal{J}(\omega)}{\omega^2}\tanh\left(\frac{\hbar\omega}{4k_BT}\right), \tag{11}$$

where k_B is the Boltzmann constant and T is the temperature. All the above three quantum reorganization energies approach λ in the classical limit, where $\hbar\omega \ll k_BT$ for all values of ω making non-negligible contributions to the integration.

Under the assumption that CT between neighboring sites occurs much more slowly than the relaxation time of molecular vibrations, contributions of nonequilibrium effects and quantum coherence can be ignored. Then, for the microscopic model Hamiltonian of Eq. (6), the CT rate between n and $m = n \pm 1$ (except for $n = 1$ or N, where only $k_{1\to2}$ and $k_{N\to N-1}$ are defined, respectively) is given by the following FGR expression:

$$k_{n\to m}^{FG} = \frac{J^2}{\hbar^2}\int_{-\infty}^{\infty} dt\exp\left(-\frac{i}{\hbar}\Delta G_{mn}t - (\mathcal{K}(0)-\mathcal{K}(t))\right), \tag{12}$$

where ΔG_{mn} has been defined by Eq. (4) and $\mathcal{K}(t)$ is the bath correlation function defined as

$$\mathcal{K}(t) = \frac{1}{\pi\hbar}\int_0^\infty d\omega\frac{\mathcal{J}(\omega)}{\omega^2}\left(\coth\left(\frac{\hbar\omega}{2k_BT}\right)\cos\omega t - i\sin\omega t\right). \tag{13}$$

The above FGR rate expression depends on the specific realization of the disorder ξ through ΔG, but this dependence is not shown explicitly. The same is true for all the approximate expressions shown below.

It is well known that the Marcus rate[40,41] (in the nonadiabatic limit) can be obtained by taking the classical bath limit of the FGR expression, Eq. (12), and can be expressed as

$$k_{n\to m}^{M} = \frac{J^2}{\hbar^2}\sqrt{\frac{\pi\hbar^2}{k_BT\lambda}}\exp\left(-\frac{(\Delta G_{mn}+\lambda)^2}{4\lambda k_BT}\right). \tag{14}$$

On the other hand, taking the short time quadratic expansion of the exponent in Eq. (12) with respect to t, one can obtain the following semiclassical (SC) approximation:[42]

$$k_{n\to m}^{SC} = \frac{J^2}{\hbar^2}\sqrt{\frac{\pi\hbar^2}{k_BT\lambda_{q,c}}}\exp\left(-\frac{(\Delta G_{mn}+\lambda)^2}{4k_BT\lambda_{q,c}}\right), \tag{15}$$

where $\lambda_{q,c}$ is defined by Eq. (9). The above expression approaches the Marcus rate expression in the high temperature limit where $\lambda_{q,c}$ becomes λ. For this reason, the SC approximation has often been regarded as the standard intermediate step for deriving the Marcus rate from the FGR rate expression. However, it is important to note that there can be significant discrepancy between λ and $\lambda_{q,c}$ even at room temperature if the contribution of high frequency molecular vibrational modes becomes significant in the environmental response of CT. In this case, the SC approximation turns out to be even worse[32] than the Marcus rate for some values of ΔG.

Another way of understanding the SC approximation is to recognize that it amounts to a stationary phase approximation of the integral in FGR for $\Delta G_{mn} = -\lambda$ only. Thus, for other values of ΔG, its accuracy is expected to degrade to the degree that it is even worse than that of the Marcus rate, which can still be viewed as a classical limit of another proper stationary phase approximation. The SPI approximation[32] improves the SC approximation in this respect

Published under license by AIP Publishing

by interpolating stationary phase approximations at three values of $\Delta G_{mn} = 0, \pm\lambda$ and is given by the following expression:

$$k_{n\to m}^{spi} = \frac{J^2}{\hbar^2}\sqrt{\frac{\pi\hbar^2}{k_B T\lambda_{q,c}U_{nm}}}\exp\left(-\frac{(\Delta G_{mn}+\lambda)^2}{4k_B T\lambda_{q,c}}\right), \tag{16}$$

where

$$U_{nm} = \left[\left(1-\frac{\lambda_{q,s}}{\lambda_{q,c}}\right)\left(\frac{\Delta G_{mn}}{\lambda}\right)^2 + \frac{\lambda_{q,s}}{\lambda_{q,c}}\right]\left(1+\alpha e^{\gamma\Delta G_{mn}/\lambda}\right). \tag{17}$$

In the above expression,

$$\alpha = \exp\left(\frac{\lambda_{q,c}\lambda_{q,t}-\lambda^2}{2k_B T\lambda_{q,c}}\right) - 1, \tag{18}$$

$$\gamma = \ln\left[\exp\left(\frac{2\lambda(\lambda_{q,c}-\lambda)}{k_B T\lambda_{q,c}}\right) - 1\right] - \ln\alpha. \tag{19}$$

The SPI approximation given above remains very close[32] to the FGR rate as long as $|\Delta G| \le \lambda$ and is thus superior to the SC approximation. However, it is important to note that $k_{n\to m}^{spi}$ does not satisfy the normalization condition with respect to the integration over ΔG_{mn} unlike the Marcus expression or the SC approximation.

The MA expression,[39] which was originally designed for the inorganic material, is different from the rate expressions presented above in that it is specifically based on the assumption of weak electron–phonon coupling. It has also been used for organic materials[39] although it cannot, in general, account for the polaronic effect[56] that is believed to be important. The MA rate is expressed as

$$k_{n\to m}^{MA} = k_0\exp\left(-\frac{\Delta G_{mn}}{2k_B T} - \frac{|\Delta G_{mn}|}{2k_B T}\right), \tag{20}$$

where k_0 decays exponentially with hopping distance but its detailed form remains ambiguous otherwise. In the present work, we define k_0 such that the resulting MA rate agrees with the Marcus rate for $\Delta G_{mn} = \pm\lambda$. Thus, it is assumed to have the following form:

$$k_0 = \frac{J^2}{\hbar^2}\sqrt{\frac{\pi\hbar^2}{k_B T\lambda}}. \tag{21}$$

All the rate expressions described above can be used for any kind of bath spectral density. However, in the present work, we focus our attention on the following Ohmic spectral density with exponential cutoff:

$$\mathcal{J}(\omega) = \pi\hbar\eta\omega e^{-\omega/\omega_c}. \tag{22}$$

This is, in fact, equivalent to the bath spectral density used in a previous,[33] and the difference in the form is due to different definitions of the bath spectral density.

C. Initial condition and physical observables

Initially, the charge carriers are located at the center site and allowed to evolve to both sides. In all our simulations, we assume that $N = 201$ and that $r_n = n\cdot dr$ for $n = 1, \ldots, N$. Thus, the initial site of the population is $n_0 = 101$. The solution of the PME for each realization of the disorder provides time dependent population $P_n(t)$, which can be used to calculate all other physical observables. The quantity of particular interest is the time dependent square displacement $R^2(t)$ defined as follows:

$$R^2(t) = \sum_{n=1}^{N} P_n(t)(r_n - r_{n_0})^2. \tag{23}$$

The average of the above expression over the ensemble of N_G sets of the disorder in G_n's, namely, the mean square displacement, is denoted as $\langle R^2(t)\rangle$. Note that each set of the disorder in site energies corresponds to a different ξ specifying H_ξ in Eq. (6). For normal diffusion, the time derivative of this approaches a steady state limit, which can be used to determine the one-dimensional diffusion constant as follows:

$$D = \lim_{t\to\infty}\frac{\mathrm{d}\langle R^2(t)\rangle}{2\mathrm{d}t} \approx \left.\frac{\mathrm{d}\langle R^2(t)\rangle}{2\mathrm{d}t}\right|_{t=t_s}, \tag{24}$$

where t_s is a large enough time for which the steady state behavior is observed.

The charge mobility (μ) is one of the most significant physical observables in characterizing CT processes and depends on details constituting molecules and their packing pattern. In our model, these effects are incorporated into hopping rates and disorder. In the limit where the applied field is vanishingly small, the following Einstein–Smoluchowski expression for the mobility can be used:

$$\mu_{ES} = \frac{eD}{k_B T}. \tag{25}$$

The above expression can be explained in terms of the linear response theory.[46] On the other hand, according to the original definition of drift mobility, one can determine the mobility in terms of the following definition directly:

$$\mu_d = \frac{v_F}{F}, \tag{26}$$

where v_F is the drift velocity resulting from the presence of the gradient. In the above equation, the drift velocity can be calculated directly from the distributions by the following relationship:

$$\langle R(t)\rangle_F = \langle R(t)\rangle_{F=0} + v_F t, \tag{27}$$

where $\langle R(t)\rangle_F$ and $\langle R(t)\rangle_{F=0}$ are ensemble averages of the travel distance, defined by an expression similar to Eq. (23) with $(r_n - r_{n_0})$ instead of $(r_n - r_{n_0})^2$. The subscripts F and $F = 0$ represent that these are calculated in the presence and absence of the gradient F, respectively. When there is a weak gradient, the drift of charges is expected to be linearly dependent on the field. However, as the field (gradient of site energies in our model) increases, the dependence on the field becomes nonlinear, resulting in the deviation of Eq. (25) from Eq. (26).

D. Units and computational methods

In numerical calculations, we adopt the same units as the previous work.[33] Namely, we use e as the unit charge, use the nearest neighbor distance $r_{n,n-1}$ as the unit distance, and assume that $\hbar = 1$.

Published under license by AIP Publishing

TABLE I. Example values of unit energy, time, and mass in rationalized units assuming the unit length $r_{n,n=1}$ = 1 nm. Corresponding values of $\kappa = J^2/(\lambda\hbar)$ assuming J = 0.01 eV are also shown.

λ (eV)	M_u (kg)	T_u (s)	κ (s^{-1})
0.025	2.776×10^{-30}	2.633×10^{-14}	6.076×10^{12}
0.1	6.941×10^{-31}	6.582×10^{-15}	1.519×10^{12}
0.5	1.388×10^{-31}	1.316×10^{-15}	3.038×10^{11}

These units are similar to atomic units but are more flexible, capable of representing multiple situations. For example, let us assume that $r_{n,n-1}$ = 1 nm in rationalized units. Then, if our unit mass and unit time are M_u (kg) and T_u (s), respectively, in rationalized units, the condition of $\hbar = 1$ implies that $M_u/T_u = 1.054\,57 \times 10^{-16}$ kg/s. In order to further simplify calculations, we also assume that $\eta = 1$ and $\omega_c = 1$ for the spectral density [Eq. (22)]. This amounts to using λ as the unit of energy and assuming that $\lambda = \hbar\omega_c$. This latter condition puts restriction on the scope of the parameters for the bath spectral density and can be removed if more general consideration is necessary. Table I provides some example values for the units of our calculation expressed in conventional units. In addition, we also assume that the nearest neighbor electronic coupling, J = 1. Although this appears to be inconsistent with the assumption of hopping mechanism, which requires a small value of J, this, in practice, amounts to dividing the actual rates with a uniform factor of $\kappa = J^2/(\hbar\lambda)$. In other words, the values of rates being calculated here can be viewed as dimensionless ones that need to be multiplied with κ. Example values of κ assuming J = 0.01 eV are provided in Table I.

We directly solve the PME [Eq. (5)] with two different methods, a fourth order Runge–Kuta (RK4) algorithm[43] and direct numerical diagonalization of the rate matrix. The latter provides a reliable validation of the results of the former. We also test the simulation of the PME results with a KMC method, which can be used for larger scale systems for which even RK4 cannot be used. Detailed description of these three methods is provided in the Appendix. For the time step of the RK4 method, we use dt = 0.1. This choice gives accurate enough results that are virtually identical to those based on direct diagonalization, as will be shown below. For the KMC simulation, we chose the size of the ensemble of random walkers to be a million, which resulted in satisfactory convergence.

III. RESULTS

A. Mean square displacements

For three representative values of temperature, k_BT = 10, 1, and 0.1, we compared the three methods for solving the PME. Note that the actual values of temperature depend on the value of λ, which serves as the unit of energy. Among all the cases of σ and F we have tested, we here provide most detailed results for the case where σ = 0.2 and F = 0 or 0.1 as this choice exhibits fairly diverse qualitative behavior. Thus, these values of σ and F are assumed implicitly except for cases where we provide results for other values for further illustration of the effects of disorder and gradient in energy.

Figure 1 shows the mean square displacements when the exact numerical evaluation of the FGR rate is used as the hopping rate. The size of the ensemble of disorder N_G was chosen to be 4000, which we found to result in satisfactory convergence. The results obtained by the three different methods, RK4, direct diagonalization, and KMC methods for solving the PME, are shown to agree very well. We could see a similar level of agreement for other rate expressions and values of σ. Thus, hereafter, we show only results calculated by the RK4 method as representative ones.

Figure 2 compares results calculated by employing different approximations for the hopping rates at k_BT = 10. We used a little larger value of N_G = 5000, in order to further ensure the convergence. The same value of N_G is used for all the following calculations.

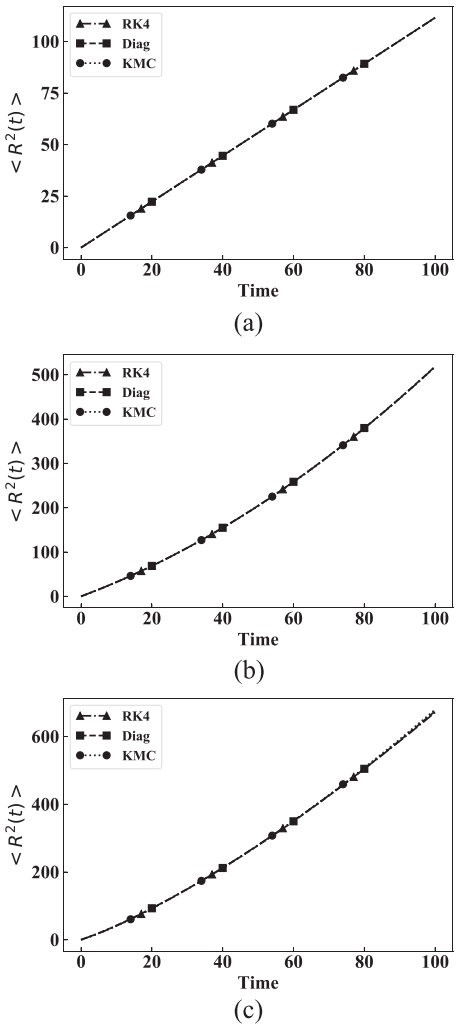

FIG. 1. Time dependent mean square displacements for σ = 0.2 and F = 0.1, at three different values of temperature, (a) k_BT = 10, (b) k_BT = 1, and (c) k_BT = 0.1. All the calculations are based on the exact numerical calculation of the FGR expression for the hopping rate. All the results calculated by the three methods, RK4, direct diagonalization, and KMC methods for solving the PME, are shown.

Published under license by AIP Publishing

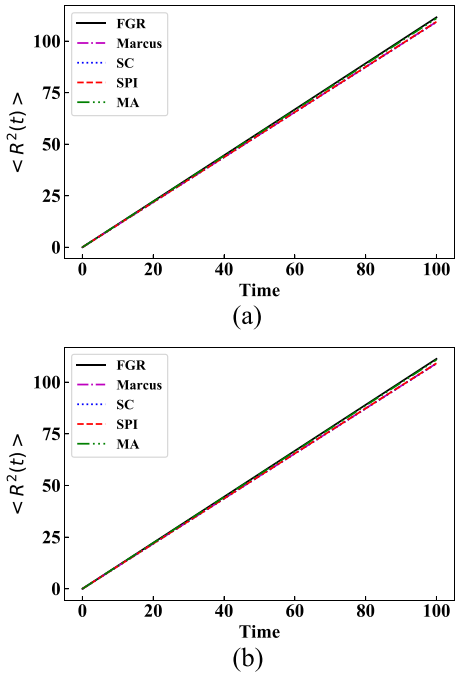

FIG. 2. Time dependent mean square displacements for $k_BT = 10$ and $\sigma = 0.2$, for (a) $F = 0$ and (b) $F = 0.1$. Results for five different rate expressions, FGR, SPI, SC, Marcus, and MA rates, are compared.

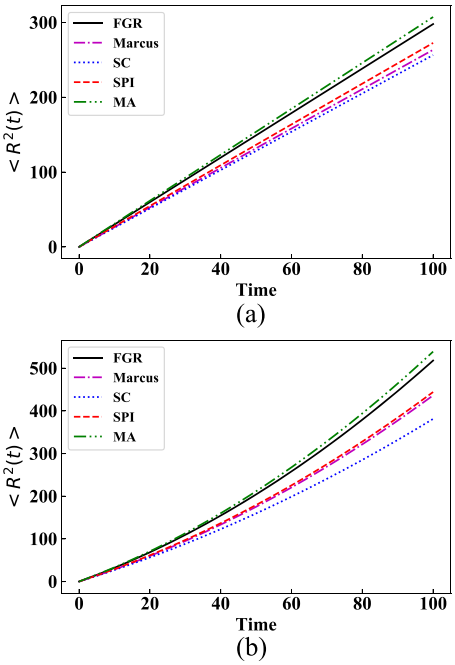

FIG. 3. Time dependent mean square displacements for $k_BT = 1$ and $\sigma = 0.2$, for (a) $F = 0$ and (b) $F = 0.1$. Results for five different rate expressions, FGR, SPI, SC, Marcus, and MA rates, are compared.

This case corresponds to a high temperature regime where the dynamics is dominated by the thermal effects of the classical bath. The choice of $\sigma = 0.2$ and $F = 0.1$ in this case amounts to weak disorder and perturbation limit. Therefore, $\langle R^2(t)\rangle$ in panel (b) is almost identical to that of panel (a). In both cases, all the approximations produce results that are very close to those of the FGR rate. It is also interesting to see that the MA expression, with the choice of Eq. (21) for k_0, now produces fairly accurate results, unlike in the previous case[33] where no such adjustment has been made. As will be shown below, this good performance is not limited to the high temperature limit.

The results for intermediate temperature, $k_BT = 1$, are shown in Fig. 3. In this case, there are significant quantum effects as can be seen from the fact that the FGR results are distinctively different from those of approximate ones. The qualitative change in the dynamics due to the presence of the gradient ($F = 0.1$) is also apparent. All the values of $\langle R^2(t)\rangle$ exhibit mildly quadratic dependence on time, indicating deviation from the normal diffusion behavior. For both $F = 0$ and $F = 0.1$, the order of performance among the three approximations of FGR is as follows: SPI > Marcus > SC, which all underestimate the results of FGR. It is worth noting that the Marcus rate performs even better than the SC approximation. On the other hand, the performance of the MA rate, the results of which slightly overestimate those of the FGR rate, is surprisingly good despite its empirical nature.

The results for low temperature, $k_BT = 0.1$, are provided in Fig. 4, which demonstrate the sensitivity of the hopping dynamics

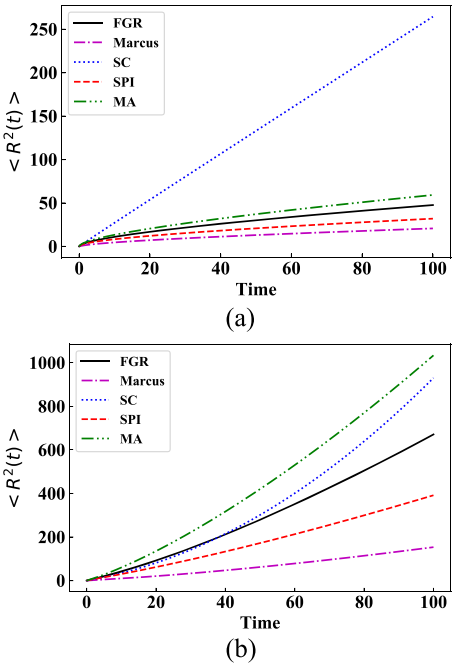

FIG. 4. Time dependent mean square displacements for $k_BT = 0.1$ and $\sigma = 0.2$, for (a) $F = 0$ and (b) $F = 0.1$. Results for five different rate expressions, FGR, SPI, SC, Marcus, and MA rate expressions, are compared.

Published under license by AIP Publishing

to the gradient and the disorder in this quantum limit. The non-diffusive behavior caused by the presence of the gradient is also significant. The sensitivity of the dynamics to the accuracy of the hopping rate is also clear. In all the cases, the results of the SPI approximation remain closer to the FGR results than those based on the Marcus rate. The performance of the SC approximation is inconsistent and even worse than that in Fig. 3. This reflects the general trend that the SC approximation significantly overestimates the effects of quantum bath and the energy gradient. While the MA rate results overestimate the FGR results, the extent of their deviation is comparable to that of the SPI approximation in this case.

It is important to note that the definition of low temperature is relative to the classical reorganization energy λ. Therefore, for the case where $\lambda = 0.26$ eV, which is not unusual, $k_BT = 0.1$ corresponds to 300 K. Thus, this is a quite plausible case, and it is worthwhile to consider additional examples of disorder. Figure 5 shows results for very low disorder ($\sigma = 0.01$) and Fig. 6 those for substantial disorder ($\sigma = 0.5$), which altogether demonstrate the sensitivity to the magnitude of the disorder in this quantum regime. Note that the saturations that are seen in Fig. 5 are due to the finite size of the system. For low disorder ($\sigma = 0.01$), there is significant quantum enhancement as can be seen from the discrepancy between the results for the FGR and Marcus rates. Figure 6 shows that such enhancement decreases substantially with the increase in disorder. As in previous case, the performance of the SC approximation is worse than others. The performance of the MA rate expression has also degraded to some extent, but it is still seen to capture the qualitative behavior of the FGR results fairly well. These results show that lowering disorder has significant positive effects on enhancing quantum effects even when the CT dynamics is governed by the incoherent hopping mechanism.

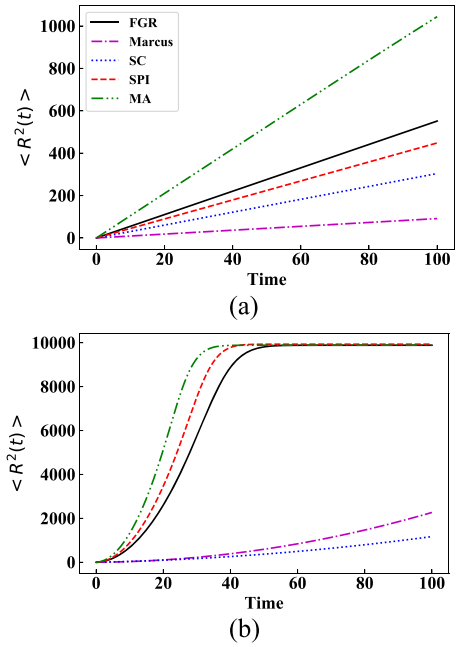

FIG. 5. Time dependent mean square displacements for $k_BT = 0.1$ and $\sigma = 0.01$, for (a) $F = 0$ and (b) $F = 0.1$. Results for five different rate expressions, FGR, SPI, SC, Marcus, and MA rate expressions, are compared.

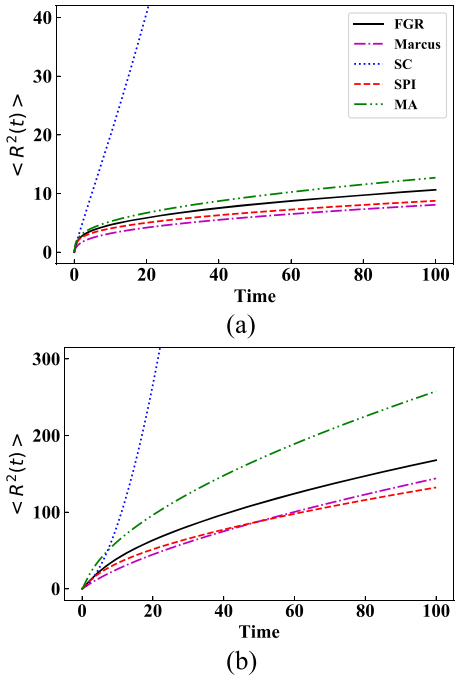

FIG. 6. Time dependent mean square displacements for $k_BT = 0.1$ and $\sigma = 0.5$, for (a) $F = 0.1$ and (b) $F = 0.5$. Results for five different rate expressions, FGR, SPI, SC, Marcus, and MA rate expressions, are compared.

B. Mobility

Given the apparent non-diffusive behavior for $F \neq 0$ except for the high temperature ($k_BT = 10$) or strong disorder ($\sigma = 0.5$) case, calculating the diffusion constant $\langle R^2(t) \rangle$ employing Eq. (24) is not appropriate in general. Despite this fact, comparison of such calculated values at specific time can be useful for comparing the extent of the spatial displacement. Figure 7 compares the resulting mobility calculated by Eq. (25) from the values of the diffusion constant evaluated by Eq. (24) at $t_s = 100$. These values of mobility remain virtually independent of the magnitude of the gradient for $k_BT = 10$. On the other hand, there is a significant nonlinear increase in the mobility with F for lower values of temperature. While these data provide quantitative means to assess the accuracy of different approximations, it is important to note that their physical meaning is unclear because the assumption of steady state limit does not hold.

Due to the difficulty in calculating the diffusion constant and the mobility by Eq. (25) for a general value of F, we tried determining the drift mobility μ_d defined by Eq. (26) directly. To this end, we have monitored all the distributions explicitly and confirmed the behavior predicted from Eq. (27). Figure 8 shows an example of population distributions illustrating this calculation method. Panel (a) shows distributions calculated by two methods for solving the PME, the RK4 and direct diagonalization methods, for $F = 0$ and $\sigma = 0.1$ at $t = 100$. These agree almost perfectly with each other, supporting the

Published under license by AIP Publishing

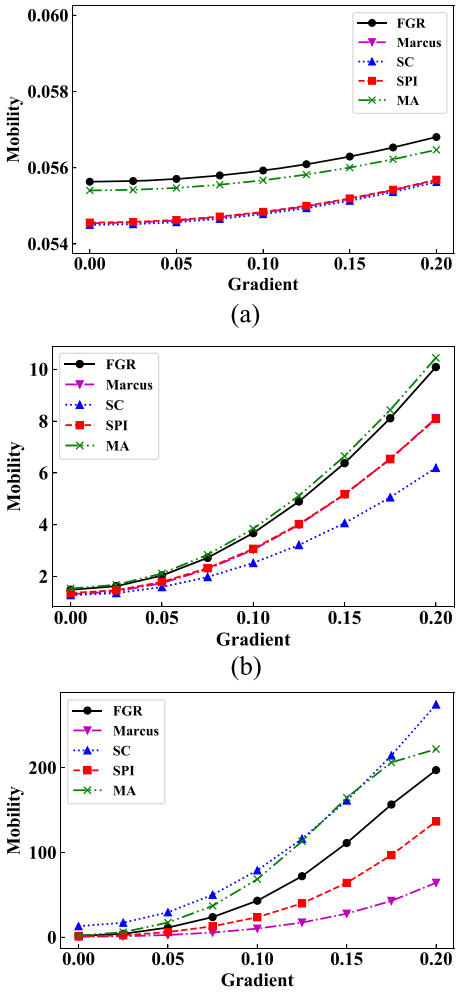

FIG. 7. Mobilities calculated by Eq. (25) in terms of D determined by Eq. (24) at $t_s = 100$ for $\sigma = 0.2$ and at three different values of temperature, (a) $k_BT = 10$, (b) $k_BT = 1$, and (c) $k_BT = 0.1$. Results for five different rate expressions are compared.

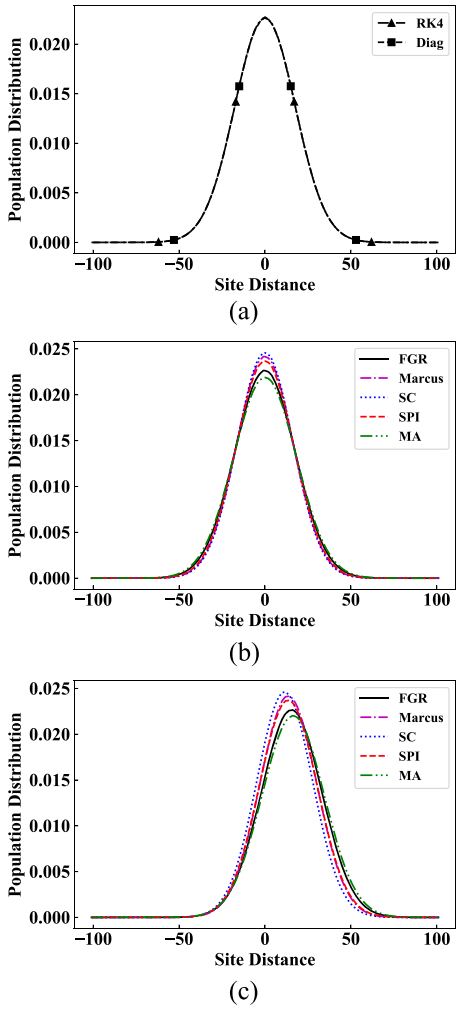

FIG. 8. 1D population distribution for temperature $T = 1$ and static disorder $\sigma = 0.1$ with $F = 0$: (a) comparison of RK4 and diagonalization methods; (b) comparison of results based on different rate expressions. (c) Comparison of populations based on different rate expressions for $F = 0.1$ at time $t = 100$.

accuracy of the RK4 method. Panel (b) shows distributions calculated employing different expressions for hopping rates and also for $F = 0$ and $\sigma = 0.1$. There are small but clear differences among those based on different rate expressions. Panel (c) shows similar results for the same conditions except that $F = 0.1$.

We have collected data similar to those shown in Fig. 8 for $\sigma = 0.2$ at the three different values of temperature varying F from 0 to 0.50 with an increment of 0.01. Figure 9 provides values of μ_d calculated directly from these distributions employing Eq. (26) for different values of the gradient F. The results for different values of temperature are shown at different panels. We confirmed that these results agree with those shown in Fig. 7 as F approaches zero. The decrease in the mobility with the increase in gradient F is due to the finite size and the boundary condition of our model. Except for a modest increase for small magnitude of the gradient at $k_BT = 0.1$, all values remain fairly insensitive to the magnitude of F until they start decreasing due to the boundary effect. We have also conducted similar calculations for $\sigma = 0.5$ at two values of $k_BT = 1$ and 0.1. The results are shown in Fig. 10. The trends here are similar to the case of $\sigma = 0.2$ except that the decrease in mobility with the increase in F here is much smaller and relative errors for the SC approximation are larger.

Figures 9 and 10 confirm that the trends of the drift mobilities calculated for different approximations are similar to those for the values of $\langle R^2(t)\rangle$. At $k_BT = 10$, all the results agree reasonably well with the exact FGR result. Both the SPI approximation and the Marcus rate are shown to work well for $k_BT = 1$, whereas the former is distinctively better than the latter at $k_BT = 0.1$. The SC approximation is unreliable in describing the temperature dependence. The

Published under license by AIP Publishing

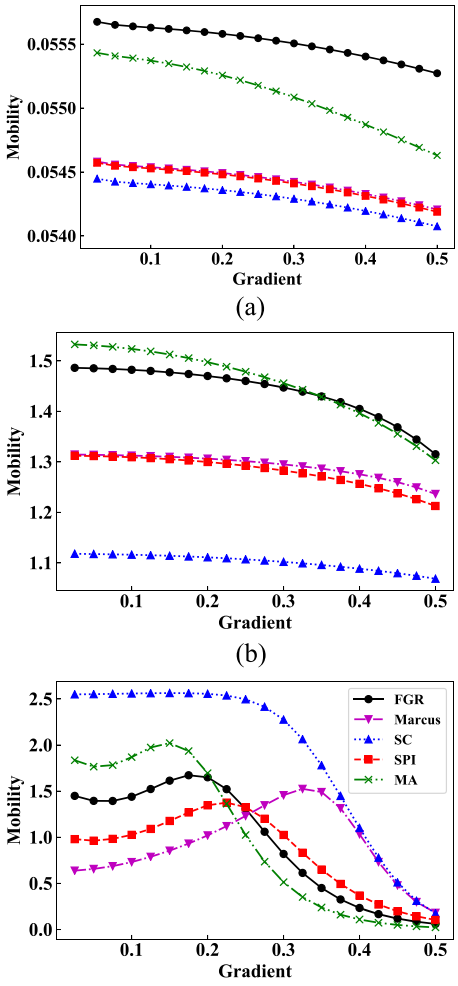

FIG. 9. Mobilities calculated by Eq. (26) at t_s = 100 for σ = 0.2 at three different values of temperature, (a) k_BT = 10, (b) k_BT = 1, and (c) k_BT = 0.1. Results for five different rate expressions are compared.

performance of the MA rate expression is surprisingly good as well although its qualitative trend is somewhat different.

The displacements of the distributions shown in Fig. 8 suggest that the non-diffusive behavior observed in Figs. 3–5 is due to the drift of distribution centers. If this is the case, $\langle R^2(t)\rangle$ should be a quadratic function of time. Indeed, we found that the time dependences of $\langle R^2(t)\rangle$ shown in Figs. 3–5 can be fitted very well by the following quadratic function of time:

$$\langle R^2(t)\rangle = v^2t^2 + 2Dt, \tag{28}$$

which is based on the assumption that there is no correlation between the drift velocity and diffusive motion. Using the value of v determined from the fitting of Eq. (28) as a drift velocity, we have determined the corresponding drift mobility according to Eq. (26).

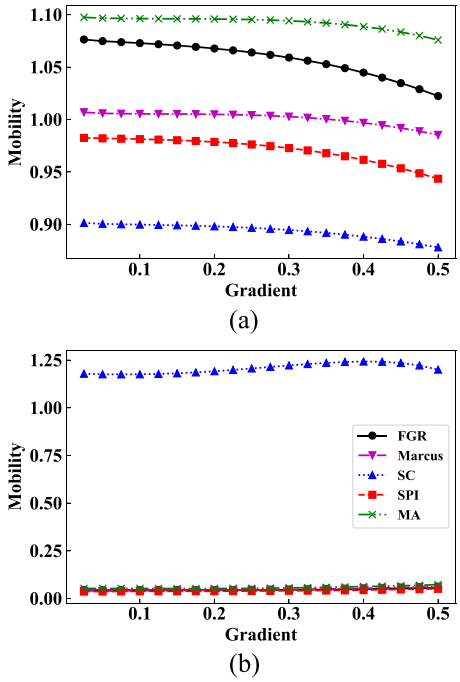

FIG. 10. Mobilities calculated by Eq. (26) at t_s = 100 for σ = 0.5 at two different values of temperature, (a) k_BT = 1 and (b) k_BT = 0.1. Results for five different rate expressions are compared.

We have also used the value of D from Eq. (28) for the determination of mobility according to Eq. (25).

Table II compares the mobilities calculated for the particular value of F = 0.1 as described above, which we denote as μ_d' and μ_{ES},

TABLE II. Values of mobilities determined from the fitting of $\langle R^2(t)\rangle$ with Eq. (28) for σ = 0.2 and F = 0.1.

Rate	k_BT	μ_d	μ_d'	μ_{ES}
FGR	1	1.48	1.48	1.49
	0.1	1.44	1.56	21.8
SPI	1	1.31	1.31	1.37
	0.1	1.03	0.993	14.7
SC	1	1.12	1.11	1.29
	0.1	2.56	2.56	13.8
Marcus	1	1.31	1.31	1.32
	0.1	0.731	0.780	4.69
MA	1	1.52	0.858	0.869
	0.1	1.87	2.04	31.4

Published under license by AIP Publishing

with those shown in Fig. 9, which have been calculated directly from distribution functions and are denoted as μ_d. The fact that the two values μ_d and μ_d' are very close to each other confirms that the source of the non-diffusive behavior is the drift motion of the distribution. For $k_BT = 1$, μ_{ES} calculated this way is also very close to the two drift mobilities. On the other hand, for $k_BT = 0.1$, where there is substantial enhancement due to quantum effects of the environment [see Fig. 9(c)], values of μ_{ES} are about an order of magnitude larger than those of μ_d and μ_d'. The source of this discrepancy is not clear at this point and requires further theoretical and computational studies, for example, based on a more general formulation of mobility.[47]

IV. CONCLUSION

In this paper, we have conducted simulations of charge hopping transport along a one-dimensional chain with Gaussian site energy disorder and uniform gradients in average energies. We compared solutions of the PME based on three different computational methods (RK4, diagonalization, and KMC). For all the cases, we found that the results of the three solution methods of PME agree satisfactorily.

Five different rate expressions, the exact evaluation of the FGR rate, the SPI approximation, the SC approximation, the Marcus rate, as in previous works,[32,33] and the MA rate, with a new prefactor given by Eq. (21), were tested. The results of this calculation clarify the capability of different approximations to represent the effects of quantum environments in the presence of energy gradients. Among all the four approximations for the rate, the SPI approximation was confirmed to work best as reported previously,[33] even in the presence of gradients. The Marcus rate works well at high temperature as expected and reasonably well at intermediate temperature with moderate quantum effects. However, it fails at low temperature where the effects of quantum environments are significant. This discrepancy is more pronounced in the presence of the energy gradient especially for weak disorder. The SC approximation, in general, performs worse than the Marcus rate. The MA rate is seen to work surprisingly well despite its empirical character.

In the presence of gradients in site energies, the dynamics, in general, becomes non-diffusive. As a result, the conventional expression for evaluating the diffusion constant, Eq. (24), cannot be used. It is not clear whether the linear response theory expression for the mobility [Eq. (25)] can be used in this case. Thus, we calculated the drift mobility [Eq. (26)] directly from the time dependent population distributions. The resulting values of mobility remain fairly insensitive to the magnitude of the gradient, except for the decrease due to the finite size of our model. We also found that the drift of the population distribution center is responsible for apparent non-diffusive behavior and that $\langle R^2(t)\rangle$ can, in general, be fitted by Eq. (28) before the boundary effect kicks in. In this fitting, the linear term represents the diffusive motion and the quadratic term the drift motion. The drift mobilities calculated in this way agreed fairly well with those calculated from the drift of distributions directly.

We found significant enhancement of the mobility due to the quantum effects of the bath, especially for non-zero F in the low temperature case of $k_BT = 0.1$ [see Fig. 5(b)]. Since this value of k_BT is relative to the reorganization energy, which can easily be ten times the room temperature thermal energy, realization of such quantum enhancement is quite plausible, especially if significant portion of the reorganization energy comes from high frequency modes, a very likely situation for materials consisting of conjugated organic molecules. Thus, our results demonstrate the feasibility of realizing significant quantum effects near room temperature even when the CT involves incoherent hopping. However, such enhancement is seen to diminish quickly even for a modest increase in disorder. As a result, quantum effects on the drift mobility, μ_d or μ_d', for $\sigma = 0.2$ are rather modest. As yet, we could identify about a factor of five enhancement for μ_{ES} as can be seen from the comparison between the FGR and Marcus rate results in Table I. The discrepancy between the two values of the mobility calls for more careful theoretical investigation of the conventional linear response theory mobility expression in the quantum regime and also for more extensive computational studies. It is also expected that the quantum effects of the bath can still be significant if additional high frequency parts representing intra-molecular vibrational modes are included. In this sense, test for more extensive set of parameters for the bath spectral density and for more complex ones with nontrivial high frequency features will be worthwhile.

Another important issue that was not clarified here but has significant implication is the dependence of mobility on the applied field, not the gradient in energy as considered here. One of the most well-known features in this regard is the Poole–Frenkel behavior,[48,49] which was originally developed based on the combination of band theory and space charge effect but then later explained also in terms of an alternative theory of correlated disorder.[50,51] The latter theory seems to explain many experimental results reporting the Poole–Frenkel behavior even when the band theory is not appropriate.[10,52–55] As yet, many microscopic details responsible for the Poole–Frenkel behavior or deviation from it are not clearly understood. One important question pertinent to this work is how the field dependence is related to the specific assumption of the hopping rate. The methods used in this work can be employed for the investigation of such details.

This work shows that the use of KMC method employing the SPI approximation and the MA rate with Eq. (21) will be useful for more comprehensive simulation study. Recent works[27–29] already showed that this approach can serve as an important component for the coarse-grained simulation of charge transport dynamics in realistic materials. A similar approach can be used for many other CT processes in complex environments.

ACKNOWLEDGMENTS

This work was supported by the U.S. Department of Energy, Office of Science, Basic Energy Sciences, under Award No. DE-SC0001393. The authors would like to thank for the computational support by the CUNY High Performance Computing Center and Queens College's Center for Computational Infrastructure for the Sciences.

APPENDIX: THREE COMPUTATIONAL METHODS

Three different methods for solving the PME [Eq. (5)] are employed and compared. A brief description of each method is provided below.

Published under license by AIP Publishing

1. Runge–Kutta method

RK algorithm[43] is a well-known method to numerically integrate the ordinary differential equation, which is an extension of Euler's method. In fact, RK refers to a class of algorithms with varying orders of accuracy and numerical overhead. One of the most widely used one is the fourth order RK method,[43] known as RK4. For a brief description of this method, let us consider the time evolution equation for $P_n(t)$ expressed as

$$\frac{dP_n(t)}{dt} = S_n(t, P_1(t), \ldots, P_N(t)), n = 1, \ldots, N. \tag{A1}$$

The PME given by Eq. (5) is a specific example of the above equation. Then, the RK4 algorithm being used in this work is represented by the following set of equations:

$$P_n(t_{k+1}) = P_n(t_k) + \frac{dt}{6}\{S_{n,1}(t_k) + 2S_{n,2}(t_k) + 2S_{n,3}(t_k) + S_{n,4}(t_k)\}, \tag{A2}$$

where dt is the time interval and

$$S_{n,1}(t_k) = S_n(t_k, \ldots, P_j(t_k), \ldots), \tag{A3}$$

$$S_{n,2}(t_k) = S_n\left(t_k + \frac{dt}{2}, \ldots, P_j(t_k) + S_{j,1}(t_k)\frac{dt}{2}, \ldots\right), \tag{A4}$$

$$S_{n,3}(t_k) = S_n\left(t_k + \frac{dt}{2}, \ldots, P_j(t_k) + S_{j,2}(t_k)\frac{dt}{2}, \ldots\right), \tag{A5}$$

$$S_{n,4}(t_k) = S_n(t_k + dt, \ldots, P_j(t_k) + S_{j,3}(t_k)dt, \ldots). \tag{A6}$$

Note that each $S_{n,p+1}(t_k)$, with $p = 1, \ldots, 3$, in the above equations requires information on $S_{n,p}(t_k)$'s for all $n = 1, \ldots, N$.

2. Direct diagonalization

The PME given by Eq. (5) can be expressed in a matrix notation as follows:

$$\frac{\mathrm{d}}{\mathrm{d}t}\boldsymbol{P} = \frac{\mathrm{d}}{\mathrm{d}t}\begin{pmatrix} P_1(t) \\ P_2(t) \\ \vdots \\ P_N(t) \end{pmatrix} = \begin{pmatrix} -\sum_{n\neq 1}^{N} k_{1\to n} & \cdots & k_{N\to 1} \\ k_{1\to 2} & \cdots & k_{N\to 2} \\ \vdots & \ddots & \vdots \\ k_{1\to N} & \cdots & -\sum_{n\neq N}^{N} k_{N\to n} \end{pmatrix}\begin{pmatrix} P_1(t) \\ P_2(t) \\ \vdots \\ P_N(t) \end{pmatrix} = \boldsymbol{K}\boldsymbol{P}. \tag{A7}$$

By diagonalizing the rate matrix $\boldsymbol{K}$, the linearly independent eigenvectors $\mathbf{v}_n$ and eigenvalues λ_n for $n = 1, \ldots, N$ can be determined. Then, the solution of Eq. (A7) is given by

$$\boldsymbol{P}(t) = \sum_{n=1}^{N} c_n e^{\lambda_n t}\mathbf{v}_n, \tag{A8}$$

where c_n's are constants determined such that $\boldsymbol{P}(0) = \sum_n c_n \mathbf{v}_n$.

3. Kinetic Monte Carlo simulation

The main idea of the KMC simulation[25,44,45] is to replace the population probability of the ensemble with an average over random walkers, each evolving probabilistically in a way consistent with the PME. Let us consider the case where a random walker has just settled at site m at time t^*. Then, the "microscopic" probability for this random walker to remain at this particular site at time $t \geq t^*$ is $p_m(t) = \exp[-k_{e,m}(t - t^*)]$, where $k_{e,m}$ is the sum of escape rates out of the site m. It is assumed here that hopping occurs only to the nearest neighbors. Thus,

$$k_{e,m} = k_{m\to m+1} + k_{m\to m-1}. \tag{A9}$$

This escape can be simulated by generating a random number ξ out of a uniform distribution between 0 and 1 and assuming that jump occurs at a specific time t satisfying the following condition:

$$t - t^* = \tau = -\frac{\ln \xi}{k_{e,m}}, \tag{A10}$$

where τ is often called the waiting time for the jump. Thus, this simulates the waiting time distribution. Since there are multiple sites to jump, completion of the hoping requires generating another independent random number. To be more specific, a new independent random number ζ is generated out of the uniform distribution between 0 and 1 so that the new site can be assigned to $m + 1$ if

$$\zeta \leq \frac{k_{m\to m+1}}{k_{m\to m+1} + k_{m\to m-1}} \tag{A11}$$

and to $m - 1$ otherwise. The above process is repeated for each random walker at each site until the sum of waiting times exceeds the total time of observation.

DATA AVAILABILITY

The data that support the findings of this study are available from the corresponding author upon reasonable request.

REFERENCES

[1] M. D. Newton, Chem. Rev. **91**, 767 (1991).
[2] M. D. Newton, Theor. Chem. Acc. **110**, 307 (2003).
[3] J. Jortner and M. Bixon, *Electron Transfer from Isolated Molecules to Biomolecules, Parts 1 and 2*, Advances in Chemical Physics Vol. 106 (John Wiley & Sons, Inc., NewYork, 1999).
[4] V. Coropceanu, J. Cornil, D. A. da Silva Filho, Y. Olivier, R. Silbey, and J.-L. Brédas, Chem. Rev. **107**, 926 (2007).
[5] N. Tessler, Y. Preezant, N. Rappaport, and Y. Roichman, Adv. Mater. **21**, 2741 (2009).
[6] O. Ostroverkhova, Chem. Rev. **116**, 13279 (2016).
[7] A. N. Aleshin, Adv. Mater. **18**, 17 (2006).
[8] A. Alverez, J. M. Costa-Fernandez, R. Pereiro, and A. Sanz-Medel, TrAC Trends Anal. Chem. **30**, 1513 (2011).
[9] O. S. Wenger *et al.*, Science **307**, 99 (2005).
[10] H. Bässler, Phys. Status Solidi (b) **175**, 15 (1993).
[11] S. Jang, T. C. Berkelbach, and D. R. Reichman, New J. Phys. **15**, 105020 (2013).
[12] K. H. Hughes *et al.*, Chem. Phys. **442**, 111 (2014).
[13] L. Wang and D. Beljonne, J. Chem. Phys. **139**, 064316 (2013).

Published under license by AIP Publishing

[14]J. E. Subotnik *et al.*, Annu. Rev. Phys. Chem. **67**, 387 (2016).
[15]L. Song and Q. Shi, J. Chem. Phys. **142**, 174103 (2015).
[16]H. Oberhofer, K. Reuter, and J. Blumberger, Chem. Rev. **117**, 10319 (2017).
[17]Y. Lin and X. Zhan, Acc. Chem. Res. **49**, 175 (2016).
[18]B. Maiti *et al.*, Chem. Sci. **8**, 6947 (2017).
[19]M. Mas-Torrent and C. Rovira, Chem. Soc. Rev. **37**, 827 (2008).
[20]K. Sun *et al.*, Nat. Commun. **6**, 6013 (2015).
[21]S. Yamamoto, Y. Maruyama, and S. Hyodo, J. Chem. Phys. **116**, 5842 (2002).
[22]M. Bouhassoune, S. L. M. V. Mensfoort, P. A. Bobbert, and R. Coehoorn, Org. Electron. **10**, 437 (2009).
[23]Y. N. Gartstein and E. M. Conwell, Chem. Phys. Lett. **245**, 351 (1995).
[24]Y. Yao, W. Si, X. Hou, and C.-Q. Wu, J. Chem. Phys. **136**, 234106 (2012).
[25]C. Groves, Rep. Prog. Phys. **80**, 026502 (2017).
[26]L. Wang *et al.*, Chem. Soc. Rev. **39**, 423 (2010).
[27]M. Sato *et al.*, IEEE Trans. Dielectr. Electr. Insul. **23**, 2978 (2016).
[28]M. Sato *et al.*, IEEE Trans. Dielectr. Electr. Insul. **23**, 3045 (2016).
[29]M. Sato *et al.*, Appl. Phys. Lett. **110**, 092903 (2017).
[30]N. J. van der Kaap *et al.*, Phys. Rev. B **93**, 140206(R) (2016).
[31]P. Siders and R. A. Marcus, J. Am. Chem. Soc. **103**, 741 (1981).
[32]S. Jang and M. D. Newton, J. Phys. Chem. B **110**, 18996 (2006).
[33]S. Jang and A. Montoya-Castillo, J. Phys. Chem. B **119**, 7659 (2015).
[34]X. Sun and E. Geva, J. Chem. Theory Comput. **12**, 2926 (2016).
[35]X. Sun and E. Geva, J. Chem. Phys. **144**, 244105 (2016).
[36]X. Sun and E. Geva, J. Chem. Phys. **145**, 064109 (2016).
[37]A. A. Kananeka *et al.*, J. Chem. Phys. **148**, 102304 (2018).
[38]J. D. Jackson, *Classical Electrodynamics* (John Wiley and Sons, Inc., New York, 1975).
[39]A. Miller and E. Abrahams, Phys. Rev. **120**, 745 (1960).
[40]R. A. Marcus, J. Chem. Phys. **43**, 679 (1965).
[41]R. A. Marcus and N. Sutin, Biochim. Biophys. Acta **811**, 265 (1985).
[42]J. J. Hopfield, Proc. Natl. Acad. Sci. U. S. A. **71**, 3640 (1974).
[43]J. D. Lambert, *Numerical Methods for Ordinary Differential Systems: The Initial Value Problem* (John Wiley & Sons, Inc., Chichester, 2002).
[44]K. A. Fichthorn and W. H. Weinberg, J. Chem. Phys. **95**, 1090 (1991).
[45]C. C. Battaile, Comput. Methods Appl. Mech. Eng. **197**, 3386 (2008).
[46]R. Kubo, J. Phys. Soc. Jpn. **12**, 570 (1957).
[47]Y. Roichman and N. Tessler, Appl. Phys. Lett. **80**, 1948 (2002).
[48]J. Frenkel, Phys. Rev. **54**, 647 (1938).
[49]J. L. Hartke, J. Appl. Phys. **39**, 4871 (1968).
[50]S. V. Rakhmanova and E. M. Conwell, Appl. Phys. Lett. **76**, 3822 (2000).
[51]W. F. Pasveer *et al.*, Phys. Rev. Lett. **94**, 206601 (2005).
[52]P. W. M. Blom and M. C. J. M. Vissenberg, Phys. Rev. Lett. **80**, 3819 (1998).
[53]D. J. Pinner, R. H. Friend, and N. Tessler, J. Appl. Phys. **86**, 5116 (1999).
[54]B. A. Gregg, J. Phys. Chem. C **113**, 5899 (2009).
[55]L. Wang, D. Fine, D. Basu, and A. Dodabalapur, J. Appl. Phys. **101**, 054515 (2007).
[56]F. C. Grozema and L. D. A. Siebbeles, Int. Rev. Phys. Chem. **27**, 87 (2008).
[57]Y. Georgievskii, C.-P. Hsu, and R. A. Marcus, J. Chem. Phys. **110**, 5307 (1999).
[58]S. J. Jang and B. Mennucci, Rev. Mod. Phys. **90**, 035003 (2018).

Published under license by AIP Publishing